

On Unifying Video Generation and Camera Pose Estimation

Chun-Hao Huang¹ Jae Shin Yoon¹ Hyeonho Jeong^{1,2*} Niloy Mitra^{1,3} Duygu Ceylan¹

¹Adobe Research ²KAIST ³University College London

<https://paulchhuang.github.io/jog3rwebsite>

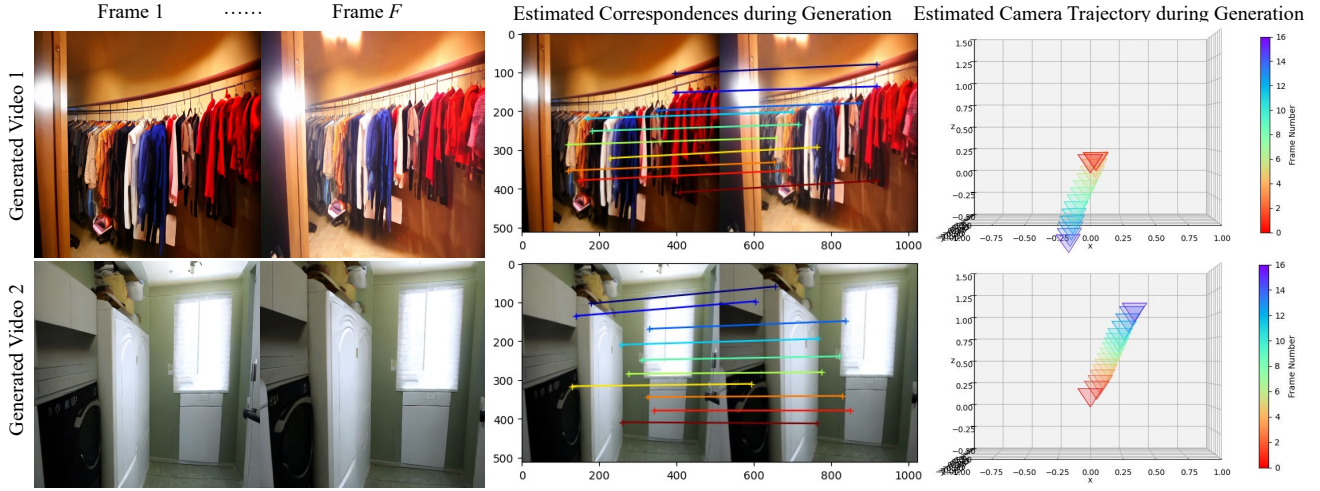


Figure 1. **JOG3R** creates realistic videos of stationary scenes while *simultaneously* generating the associated camera pose for each frame. Colors from red to purple indicate progression from the first to the last frame.

Abstract

Inspired by the emergent 3D capabilities in image generators, we investigate whether video generators similarly exhibit 3D awareness. Using structure-from-motion (SfM) as a benchmark for 3D tasks, we ask if intermediate features from OpenSora, a video generation model, can support camera pose estimation. We first examine native 3D awareness in video generation features by routing raw intermediate outputs to SfM-prediction modules like DUS3R [69]. Then, we explore the impact of fine-tuning on camera pose estimation to enhance 3D awareness. Results indicate that while video generator features have limited inherent 3D awareness, task-specific supervision significantly boosts their accuracy for camera pose estimation, resulting in competitive performance. The proposed unified model, named JOG3R, produces camera pose estimates with competitive quality without degrading video generation quality.

*Part of this work was done during the internship at Adobe Research.

1. Introduction

Building on breakthroughs in foundational image models [53], video diffusion models have advanced rapidly in recent years, resulting in numerous commercial and open-source models [5, 7, 21, 44, 87]. Trained on large-scale datasets like WebVid-10M [2] and Panda-70M [12], these models generate realistic, diverse, and temporally smooth videos from text or image prompts.

Beyond generating high-quality content, foundational generative models have recently been employed as *feature extractors*, utilizing their intermediate features to tackle various analysis tasks such as correspondence matching and semantic segmentation [17, 60]. Notably, even though trained exclusively on 2D data, image generators have demonstrated emergent abilities for 3D-aware tasks [18]. Inspired by this success, we ask if the *pre-trained video generators have similar emergent behavior towards 3D awareness*. To investigate this, we pick the classical structure-from-motion (SfM) as the target 3D task, as it requires reasoning about both scene geometry and the relative viewpoint changes across frames.

In an exciting recent development, DUS_t3R [69] demonstrated that the long-standing optimization-based structure-from-motion framework for camera estimation can be directly replaced by the forward pass of a dedicated network that has been trained to establish correspondence between any given pair of images. We observe that the ViT backbone in DUS_t3R actually shares many architectural designs in common with the Diffusion Transformers (DiT) backbone in state-of-the-art video generators. This encourages us to investigate whether the intermediate features of a DiT-based video generation model, OpenSora in our setting, can be repurposed for the task of camera pose estimation.

To facilitate our study, in this paper, we first present a novel architecture unifying video generation with camera pose estimation, which we refer to as *JOint Generation and 3D camera Reconstruction*, in short JOG3R. In particular, we attach DUS_t3R like prediction modules to a video generation network which are responsible for camera pose estimation. Being a unified model, JOG3R can generate videos (T2V), estimate camera poses given a video (V2C), or do both in one go (T2V+C). We perform a thorough study on both tasks under the JOG3R framework. We first explore if video generator features natively have 3D awareness by routing raw intermediate features from the pre-trained video generator to the camera pose estimation prediction heads. We then investigate whether the features can be further adapted towards camera pose estimation. In particular, we test whether with fine-tuning one can produce video generator features that can also be reused for improved camera tracking. Finally, we analyze the effect of such fine-tuning on generation quality. Our experiments show that while video generation features exhibit some 3D awareness natively (*i.e.*, obtained from pre-trained generator directly), adapting them with additional supervision on the camera pose estimation task significantly boosts their 3D awareness. This additional supervision produces competitive camera pose estimations compared to state-of-the-art solutions without resulting in quality degradation in generated videos.

In summary, our contributions include:

- Extensive experimentation and study on how well the video features can be used for 3D camera estimation and ablating the various design choices.
- The first unified model that can both generate videos and estimate 3D cameras (see Figure 1). We refer to this model as *JOint Generation and 3D camera Reconstruction* network, in short JOG3R.

2. Related Work

2.1. Diffusion-Based Video Generation

Building on the success of diffusion models [27, 58] in image synthesis [15, 53], the research community has ex-

tended diffusion-based methods to video generation. Early works [28, 29] adapted image diffusion architectures by incorporating a temporal dimension, enabling the model to be trained on both image and video data. Typically, U-Net-based architectures incorporate temporal attention blocks after spatial attention blocks and 2D convolution layers are expanded to 3D convolution layers by altering kernels [29, 75]. Latent video diffusion models [5, 6, 24, 67] have been introduced to avoid excessive computing demands, implementing the diffusion process in a lower-dimensional latent space. Seeking to generate spatially and temporally high-resolution videos, another line of research adopts cascaded pipelines [3, 28, 57, 71, 82], incorporating low-resolution keyframe generation, frame interpolation, and super-resolution modules. To maximize computational scalability, recent waves in video generation [7, 11, 42, 44, 87] diverge from U-Net-based architecture and employ the Diffusion Transformer (DiT) [49] backbone that processes space-time patches of video and image latent codes. Following this direction, we build our method on OpenSora [87], a publicly available DiT-based latent video diffusion model.

2.2. 3D Reconstruction

The fundamental principles of multiview geometry [73] including feature extraction [8, 40], matching [1, 22, 39, 74], and triangulation with epipolar constraints are well known to produce highly accurate (yet sparse) 3D point clouds with precise camera pose estimation from multiview images [55]. The efficiency of 3D reconstruction has been improved with linear-time incremental structure-from-motion [74] and coarse-to-fine hybrid approaches [13, 14]. To improve robustness to outliers, researchers proposed global camera rotation averaging [14], camera optimization techniques based on features of points vanishing with oriented planes [30] or from a learned neural network [37] to prevent rotation and scale drift issues. Global camera pose registration and approximation with geometric linearity [10, 32] or joint 3D point position estimation [48] are designed to further push the scalability and efficiency of the 3D reconstruction as well as the robustness particularly to the image sequence with small baselines.

Given estimated camera poses and sparse 3D point clouds, multiview stereo can then produce a dense 3D surface using hand-created visual features [56] or neural features with a cost volume [43, 43, 62, 77, 85] to predict globally coherent depth estimates. Existing neural rendering methods reconstruct such a dense surface by modeling the implicit or explicit cost volume and differentiable rendering of the scene for photometric supervision from multiview images [20, 36, 45, 46, 50, 59, 68, 70, 79] or monocular depth estimation [54]. Some pose-free methods further erase the requirement of camera calibration: test time

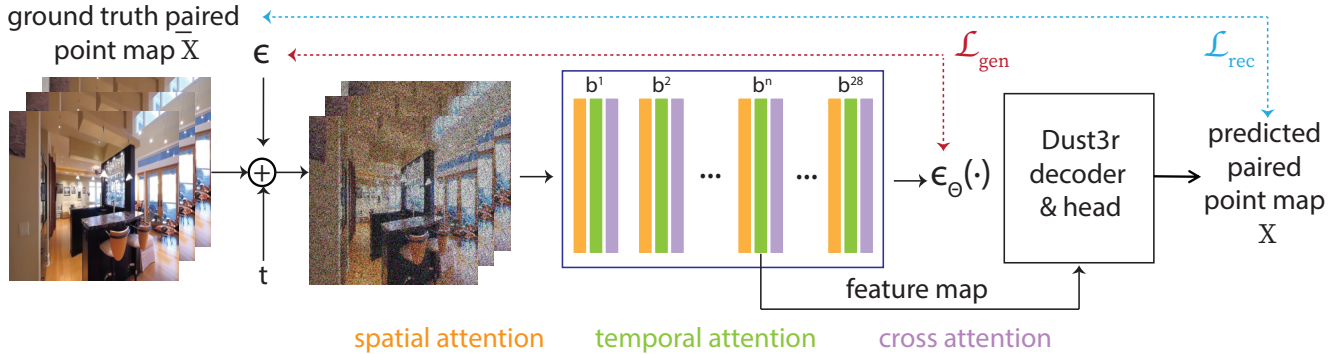


Figure 2. We propose a unified framework to investigate if the intermediate features from a video generation model can be repurposed for camera pose estimation by routing them to the SoTA camera calibration decoder of DUST3R. We investigate the effect of freezing vs training certain modules of the generator using different combination of generation and reconstruction losses.

optimization produces globally consistent depth map under unknown scale and poses using frozen depth prediction model [76]; the unsupervised signals from dense correspondences such as optical flow are integrated to learn from unlabeled data [61, 78, 88]. Recent works proposed a direct regression framework for dense surface reconstruction from pairwise images by learning to predict globally coherent depths and camera parameters [63] or to directly predict per-pixel 3D point clouds from two views [34, 69] using a vision transformer with dense tokenization techniques [52].

2.3. Diffusion Model as Features for Reconstruction

A generative diffusion model is often trained on millions of paired image and text prompts and in the process develops a semantically meaningful visual prior. Naturally, researchers are interested in using this strong prior for many downstream 3D vision tasks. Injecting 3D awareness into the diffusion prior greatly improves the accuracy and generalizability of the monocular depth estimation and correspondence search tasks [18, 80]. The latent features from the frozen pretrained diffusion model are often used as a backbone, and a task-specific decoder with cross attention is newly trained for semantic correspondences [25, 25, 31, 60, 83, 84], 3D correspondences [17], semantic segmentation and monocular depth estimation [86], material and shadow prediction [81], general object 3D pose estimation [9, 47]. However, such image diffusion features do not inherently consider the temporal relation between the frames, leading to temporally unstable 3D prediction results from videos. In contrast, we propose to utilize the video diffusion features as a backbone for the multitasking prediction of video generation and 3D camera poses estimation.

3. Method

3.1. Model and Preliminaries.

Video diffusion model. We consider OpenSora [87] as our base video generation model, which is a DiT-based video diffusion model inspired by the notable success of Sora [7]. It performs the diffusion process in a lower-dimensional latent space defined by a pre-trained VAE encoder \mathcal{E} . Each frame x of the input video is first projected into this latent space, $z_0 = \mathcal{E}(x)$. Given a diffusion time step t , the *forward* process incrementally adds Gaussian noise to the latent code z_0 via a Markov chain and obtains noisy latent z_t . The denoising model ϵ_θ takes the noisy latents of all frames, the time step t , and the text prompt y as input to predict the added noise: $\epsilon_\theta(\{z_t^f\}_{f=1}^F, t, y)$, where F is the total number of frames and θ denotes the parameter of the DiT network [49]. The network consists of 28 spatial-temporal diffusion transformer (STDiT) blocks $\{b^1, \dots, b^{28}\}$, similar to [42]. The iterative process of noise prediction and noise removal is referred to as the *reverse* process.

Camera pose estimation module. We employ the state-of-the-art multi-view stereo reconstruction (MVS) framework DUST3R [69], as our camera tracking module. Given an image pair, DUST3R encodes each image independently with a ViT encoder [16, 72]. Two decoders process both features to enable cross-view information sharing, followed by separate heads that estimate point maps $X \in \mathbb{R}^{H \times W \times 3}$, represented in the coordinates of the first view as $X^{1,1}$ and $X^{2,1}$, respectively. The relative camera pose is then estimated by aligning $X^{1,1}$ and $X^{1,2}$ using Procrustes alignment [41] with PnP-RANSAC [19, 33]. A global optimization scheme is employed to register more than a pair of views from the same scene as post-processing.

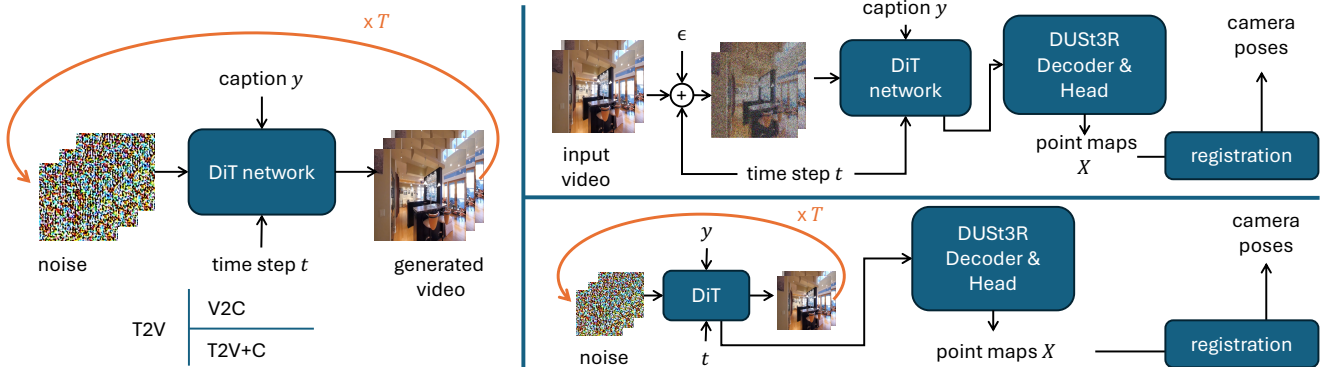


Figure 3. We base our analysis on three main tasks: text-to-video (T2V), video to camera estimation (V2C), and joint video generation and camera estimation (T2V+C) at inference time.

3.2. Unifying Video Generation and Camera Reconstruction

To facilitate our analysis, we propose a unified framework that routes intermediate features from the video generator to the camera pose estimation task. We observe that ViT and DiT share many architectural designs in common since they both belong to the broad transformer family. Hence, our key insight is to replace the *image*-based ViT encoder in DUST3R with the *video* DiT backbone in OpenSora. In this setup, we pass the intermediate features of the denoising DiT network ϵ_θ to DUST3R decoders and heads (see Figure 2 for illustration).

Specifically, we extract the output of the intermediate STDiT block b^n at a particular time step t during the reverse process. Following Tang *et al.* [60], we consider small t where the feature focuses more on low-level details, making it useful as a geometric feature descriptor to build correspondence across frames.

Our modification of DUST3R. The features extracted from the video generator encode a sequence of F frames and are provided to the DUST3R in a pair-wise manner. At training, the first frame can ideally be paired with all other frames f . In practice, due to memory constraints, we sample 4 pairs from the set $\{(1, f)\}_{f=2}^F$ to predict the 3D point maps.

At inference time, we first predict the point maps between all pairs $(1, f)$ and perform the global camera registration in DUST3R to refine the camera pose, depth and focal length for each frame, akin to bundle adjustment. Since our input is not a set of sparse views but a temporal sequence, we append two new terms, $\mathcal{L}_{\text{tranl}}$ and \mathcal{L}_{fl} , to the original global registration objective, encouraging smooth camera translation and consistent focal length between neighboring frames respectively. The two terms are used only at inference, and we refer to suppmat. for the detailed formulation.

Training objectives. For training, we consider two main training objectives, generation loss \mathcal{L}_{gen} and reconstruction loss \mathcal{L}_{rec} . The generation loss \mathcal{L}_{gen} is the common objective

in training diffusion models that aims to match the added noise ϵ . The reconstruction loss \mathcal{L}_{rec} , following the definition in DUST3R, is the sum of confidence-weighted Euclidean distance $L_2(f, i)$ between the regressed point maps X and the ground truth point maps \bar{X} over all valid pixels i and all frames f . Formally,

$$\mathcal{L}_{\text{gen}} = \left\| \epsilon - \epsilon_\theta \left(\{z_t^f\}_{f=1}^F, t, y \right) \right\|_2^2 \quad (1)$$

$$\mathcal{L}_{\text{rec}} = \sum_{f \in \{2, \dots, F\}} \sum_i C_i^{f,1} L_2(f, i) - \alpha \log C_i^{f,1} \quad (2)$$

$$L_2(f, i) = \left\| \frac{1}{s} X_i^{f,1} - \frac{1}{\bar{s}} \bar{X}_i^{f,1} \right\|_2$$

where the scaling factors s and \bar{s} handles the scale ambiguity between prediction and ground-truth by bringing them to a normalized scale, $C_i^{f,1}$ is the confidence score for pixel i which encourages network to extrapolate in harder areas, and α is a hyper-parameter controlling the regularization term [65]. We refer interested readers to [69] for more details. In our experiments, we study the effect of different combination of these two losses. Specifically, activating \mathcal{L}_{rec} alone analyzes the native 3D awareness of the video generation features while using them in conjunction, $\mathcal{L}_{\text{total}} = \mathcal{L}_{\text{gen}} + \lambda \mathcal{L}_{\text{rec}}$ (we empirically set $\lambda = 1$) investigates if the features can further be adapted for both video generation and camera pose estimation tasks. In our experiments, the video generation model is pre-trained while the DUST3R decoder and heads attached to this generation model are trained from scratch.

Inference. We base our analysis on evaluations conducted on three specific tasks (see Fig. 3 and supplemental video). (i) *Video-to-camera (V2C)*: We add noise to a given input video based on a sampled time step t , denoise it for one time step, route the feature maps to DUST3R decoders and heads, followed by registration of point maps X to

obtain camera poses. (ii) *Text-to-video (T2V)*: We evaluate the effect of using additional supervision from camera pose estimation on generation quality for the task of text to video generation where we sample Gaussian noise and iteratively denoise it with the text guidance. (iii) *Text-to-Video+Camera (T2V+C)*: Once trained with a combination of generation and reconstruction losses, the proposed unified JOG3R framework can be used to perform text-to-video generation while simultaneously routing the intermediate features to the reconstruction module at the desired time step, without the overhead of adding noise and passing it through the network again. As a result, cameras are generated alongside the video *in one go*.

Implementation details. We adopt OpenSora 1.0 as our video generator, which uses 2D VAE (from Stability-AI) [53], T5 text encoder [51], and an STDiT (ST stands for spatial-temporal) architecture similar to variant 3 in [42] as the denoising network. Among the 28 STDiT blocks, we empirically set the first 4 frozen and update only the weights of the temporal attention layers for the remaining 24 blocks. We extract the output of the 26th block b^{26} as feature maps for DUS3R decoders. The final two blocks behave as a “generation” branch whose weights are only updated by the gradient of generation loss \mathcal{L}_{gen} . We refer to the supplementary material where we provide a thorough analysis on how the features obtained from different STDiT blocks perform.

We adopt the linear prediction head of DUS3R for final pointmap estimation. DUS3R originally uses a decoder with 12 transformer blocks that is duplicated for each of the pair of frames. However, information sharing is enabled between the two decoders. In our experiments, we find that a decoder structure with six transformer blocks provides similar performance and report our results accordingly. We note that the decoder blocks we use in our training experiments are trained from scratch. Furthermore, since the features we get from the generator encode all the frames in a video sequence, we also experiment with replacing the duplicate decoder architecture with a single decoder consisting of 6 transformer blocks that perform full 3D attention across all the frames. We empirically find that this performs on par with duplicate decoders (see Table 1), and hence we use the latter to provide a more fair comparison to DUS3R.

When training, we sample the time step $t \in [0, 10]$ (corresponding to 10% of noise level) and consider the empty prompt for computing the reconstruction loss \mathcal{L}_{rec} , while for the generation loss \mathcal{L}_{gen} we sample the full range of time steps and use the captions of the videos. At test time, we sample $t \in [0, 5]$ to add noise to the input video for camera estimation (V2C). To perform joint camera estimation and video generation (T2V+C), we run the standard T2V pipeline of OpenSora and when the time step reaches the sampled $t \in [0, 5]$, we provide the output of block b^{26} to DUS3R for camera estimation.

4. Experiments

We evaluate the design choices in two main aspects. We follow standard approaches to assess the generated video quality (T2V) while validating the accuracy of camera pose estimation on real videos (V2C). We further provide results for jointly generating videos along with camera pose estimation (T2V+C). Since there is no ground truth in this case, we focus on and report self-consistency.

4.1. Setup

Data. We choose RealEstate10K [89] as the dataset, which has around 65K video clips paired with camera parameter annotations. We use the captions of RealEstate10K provided in [23] and also follow their train/test split. As pre-processing, we pre-compute the VAE latents of the video frames and the T5 text embeddings of the captions. We sample $F=16$ frames from the original sequences with a frame stride randomly chosen from $\{1, 2, 4, 8\}$ and 0.5 probability to reverse the frame order. To obtain point map annotation \bar{X} , we estimate metric depth with ZoeDepth [4], un-project it to 3D and transform to the coordinate of the first frame using the camera parameters in RealEstate10K. All camera extrinsic parameters are expressed w.r.t. the first frame.

In addition, we consider DL3DV10K [38], which also provides camera annotations, as an additional test set. We choose a random set of 70 videos for testing and caption the first frame of each video using [35]. We prepare point map annotations using ZoeDepth [4].

Baselines. Since there is no existing method that can perform both video generation and camera pose estimation jointly, we can only compare to task-specific methods. We use the original pair-wise method DUS3R [69] with linear head and a global SfM method GLOMAP [48] as camera pose estimation methods to provide a reference for our analysis. For DUS3R we consider three variants: (i) off-the-shelf pretrained weights (DUS3R[†]), (ii) initialized with pretrained weights and trained with the same data as ours (DUS3R*), and (iii) trained from scratch with the same data as ours (DUS3R⁰). In all three variants, we perform the final global optimization step with our newly introduced temporal loss $\mathcal{L}_{\text{tranl}}$ and \mathcal{L}_{fl} . For video generation we consider the pretrained OpenSora as a baseline.

Metrics. We validate the quality of camera tracking on real videos (V2C) by comparing the estimated camera poses (\mathbf{R}, \mathbf{t}) with the ground truth poses $(\bar{\mathbf{R}}, \bar{\mathbf{t}})$. For rotation, we compute the relative error between two rotation matrices [66]. Since the estimated and ground-truth translation can differ in scale, we follow [66] to compute the angle between the two normalized translation vectors, *i.e.*, $\arccos(\mathbf{t}^\top \bar{\mathbf{t}} / (\|\mathbf{t}\| \|\bar{\mathbf{t}}\|))$. Besides reporting the average of the two errors, we also follow [69] to report Relative Rotation Accuracy (RRA) and Relative Translation Accuracy (RTA),

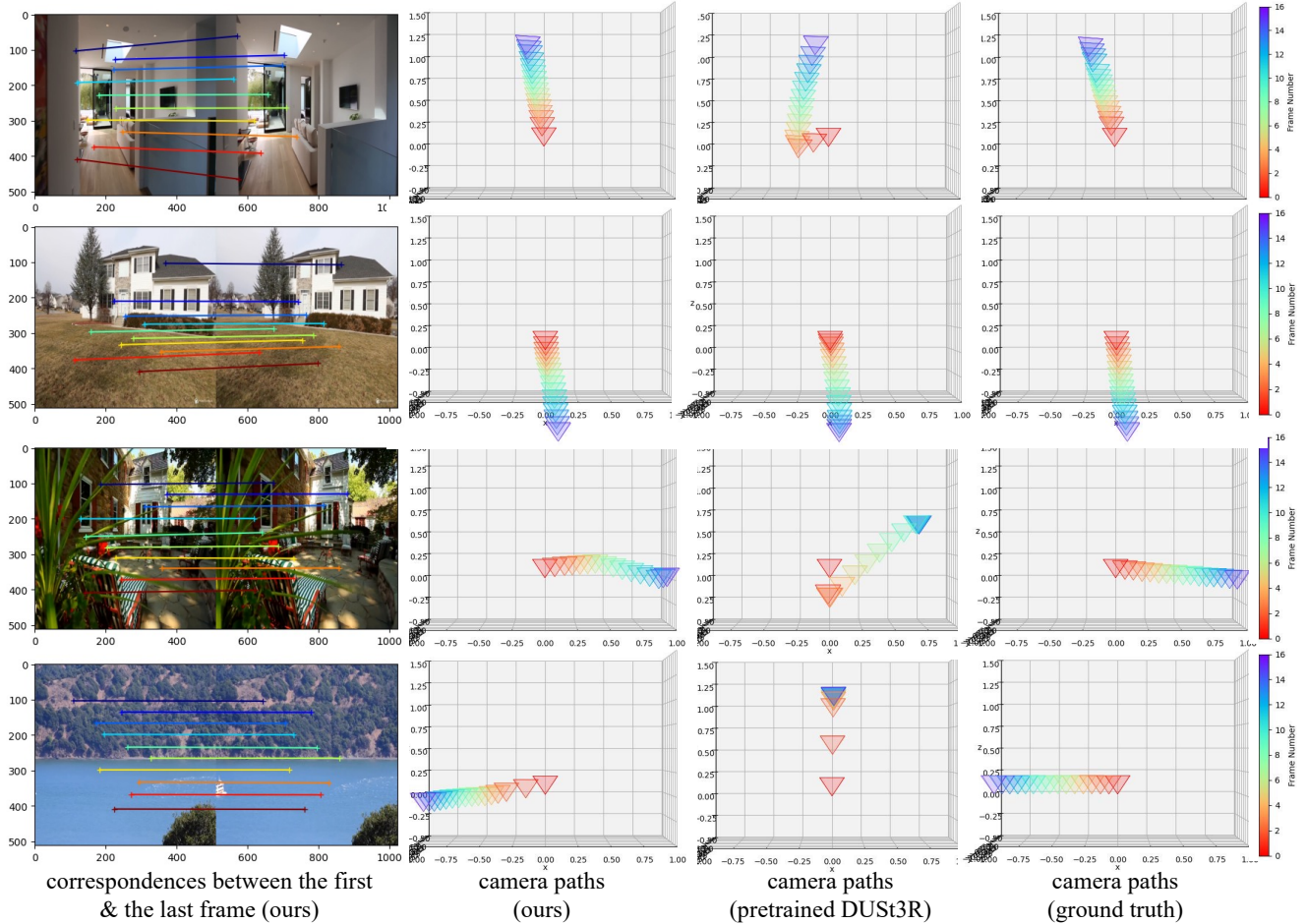


Figure 4. **Qualitative camera pose estimation (V2C) results.** Red to purple indicates the progression from the first to the last frame.

Backbone / Method	\mathcal{L}_{gen}	$\mathcal{L}_{\text{fl}} \& \mathcal{L}_{\text{tranl}}$	Rot. err. ($^\circ$) \downarrow	Transl. err. ($^\circ$) \downarrow	RRA@5 $^\circ$ \uparrow	RTA@5 $^\circ$ \uparrow	mAA@30 $^\circ$ \uparrow
1a. frozen DiT	n.a.	✓	0.40	26.72	99.80%	11.63%	38.40%
1b. trainable DiT	✗	✓	0.28	21.13	99.90%	19.23%	49.49%
1c. trainable DiT (JOG3R)	✓	✓	0.29	22.15	99.79%	19.18%	47.25%
1d. trainable DiT	✓	✗	0.37	32.66	99.77%	13.16%	35.62%
2a. DUST3R † [69]	n.a.	✗	0.77	36.61	97.56%	7.54%	30.13%
2b. DUST3R † [69]	n.a.	✓	0.53	27.86	99.12%	13.70%	40.20%
2c. DUST3R* [69]	n.a.	✓	0.23	9.17	99.90%	54.17%	75.50%
2d. DUST3R 0 [69]	n.a.	✓	0.32	20.66	99.70%	15.33%	47.47%
3. GLOMAP [48]	n.a.	n.a.	0.96	19.55	96.86%	25.92%	55.82%

Table 1. **V2C error comparison on RealEstate10K-test.** DUST3R † indicates pretrained DUST3R weights, whereas DUST3R* is further trained with the same training set as our method – RealEstate10K-train. DUST3R 0 denotes training with RealEstate10K-train from scratch without initializing with pretrained weights. **Red**: best in the sub-table; **blue**: second place in the sub-table.

i.e., the percentage of camera pairs with rotation/translation error below a threshold. Due to the small number of frames handled by the video generator, each videos sequence exhibits small rotation variation. Hence, we select a threshold 5 $^\circ$ to report RTA@5 and RRA@5. Additionally, we cal-

culate the mean Average Accuracy (mAA@30), defined as the area under the curve accuracy of the angular differences at min(RRA@30, RTA@30). We also use FID [26] and FVD [64] to measure image and video quality, respectively.

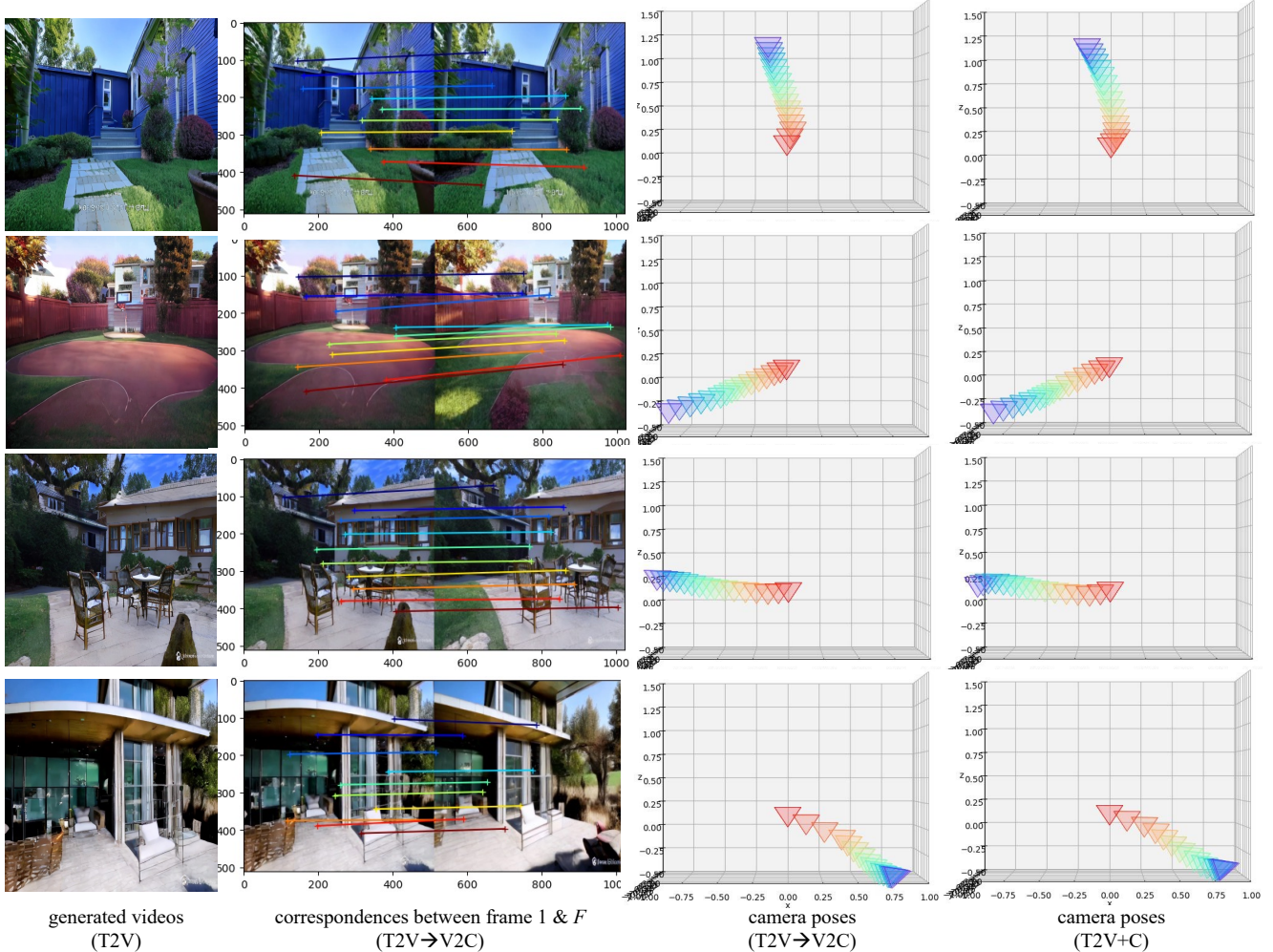


Figure 5. **Qualitative generation T2V+C results.** It is coherent with the camera paths from T2V→V2C. Please see suppmat. for videos.

Backbone / Method	\mathcal{L}_{gen}	\mathcal{L}_{fl} & $\mathcal{L}_{\text{tran}}$	Rot. err. (°) ↓	Transl. err. (°) ↓	RRA@5° ↑	RTA@5° ↑	mAA@30° ↑
1a. frozen DiT	n.a.	✓	6.49	39.53	65.06%	2.81%	19.70%
1b. trainable DiT	✗	✓	4.54	30.05	76.27%	7.88%	33.60%
1c. trainable DiT (JOG3R)	✓	✓	4.20	29.17	78.63%	7.86%	34.22%
1d. trainable DiT	✓	✗	6.94	41.11	62.43%	2.66%	17.18%
2a. DUST3R [†] [69]	n.a.	✗	1.64	20.10	96.25%	37.03%	55.97%
2b. DUST3R [†] [69]	n.a.	✓	1.33	14.75	97.53%	47.03%	65.73%
2c. DUST3R* [69]	n.a.	✓	1.83	14.17	93.63%	38.57%	64.40%
2d. DUST3R ⁰ [69]	n.a.	✓	6.25	39.37	65.84%	3.41%	19.73%
3. GLOMAP [48]	n.a.	n.a.	0.53	4.92	98.03%	87.39%	90.39%

Table 2. **V2C error comparison on DL3DV10K.** Red: best in the sub-table; blue: second place in the sub-table.

4.2. Reconstruction Evaluation

In Table 1, we compare the camera pose estimation (V2C) errors on RealEstate10K-test and report the errors of withheld DL3DV10K in Table 2. In both tables, even when there are decoders trained to perform reconstruction from

the Sora features, freezing Sora backbone still leads to noticeably worse results than the trainable counterparts (row 1a vs. 1b or 1c). This means *raw features from pretrained video generators are insufficient for camera pose estimation*. Comparing rows 1b and 1c of two tables, we see that models trained without generation loss \mathcal{L}_{gen} lead to overall

similar results to our full model, suggesting that *retaining generation ability has limited effect on reconstruction*.

Our full method, JOG3R, performs overall better than pretrained DUS_t3R[†] on RealEstate10K, cf., Table 1 row 1c and 2b. When trained with the same RealEstate10K-train, JOG3R still has on-par reconstruction quality compared with the from-scratch trained DUS_t3R⁰, but not DUS_t3R*. This suggests pretrained DUS_t3R weights contain richer information for camera pose estimation than the pretrained OpenSora weights. Meanwhile, the overall results in Table 2 suggests JOG3R is not as competitive in generalization, which we attribute to the faster motion in DL3DV10K. Since DUS_t3R[†] and DUS_t3R* contain pre-trained knowledge learned from matching wide-baseline view pairs, they naturally perform better than DUS_t3R⁰ in DL3DV10K, which is solely trained with RealEstate10K-train. We also report the results of GLOMAP [48], an optimization based state-of-the-art SFM method. In row 3 of both tables, we observe it does surpass most methods, except for DUS_t3R* in Table 1. This demonstrates the strength of the optimization-based global method.

Figure 4 shows the qualitative comparison of our method and baselines (with \mathcal{L}_{fl} & \mathcal{L}_{trans}). Since camera poses are estimated through registration, which builds 3D correspondences along the way, we visualize the final camera trajectories as well as the correspondence between the first and the last frame. One can see that our method produces good camera trajectories similar to pretrained DUS_t3R, which is a method tailored for reconstruction only, but no generation. In some cases ours are closer to ground truth camera paths.

4.3. Generation Evaluation

For each method, we generate 180 videos using the captions in RealEstate10K-test and report the FID/FVD against the real images/videos in RealEstate10K-test. Table 3 suggests that our full model generates more realistic images/videos than pretrained OpenSora (row 1c vs. 2). When ablating the generation loss \mathcal{L}_{gen} , the quality slightly degrades compared to our full model (row 1c vs. 1a). This is intuitive because without the generation loss, there is nothing to enforce the model to retain its full generation capability. See also supplemental videos. It is worth noting that row 1b corresponds to a baseline where \mathcal{L}_{rec} is disabled by removing DUS_t3R decoders/heads, i.e., it is equivalent to standard diffusion model finetuning except only the weights of the temporal attention layers are updated. We see that removing \mathcal{L}_{rec} leads to different impacts on FID and FVD. Therefore, we conclude *camera pose estimation has mixed impact on video generation*. Figure 6 shows a few examples of videos generated by JOG3R.

Backbone / Method	\mathcal{L}_{gen}	\mathcal{L}_{rec}	FID ↓	FVD ↓
1a. trainable DiT	✗	✓	94.52	1797.07
1b. finetuned OpenSora	✓	✗	88.02	1440.92
1c. trainable DiT (JOG3R)	✓	✓	79.94	1742.73
2. pretrained OpenSora	n.a.	n.a.	115.36	1872.41

Table 3. **Generation quality comparison.** We compute the FID and FVD with the RealEstate10K-test.

4.4. Discussion

Self consistency of T2V → V2C and T2V+C. Since JOG3R can *generate* camera trajectories in two ways: cascading T2V and V2C or the tightly coupled T2V+C pipeline, it is worth comparing how much the two results differ. We run the two pipelines with 100 prompts and report 0.45° average difference in rotation and 19.20° in translation; both are low errors compared with the corresponding numbers in Table 1 and 2, indicating that the camera poses from joint T2V+C pipeline is consistent with T2V → V2C. The qualitative results in Figure 5 also confirm this conclusion.



Figure 6. **Qualitative T2V generations.** Please see suppl. videos.

Synergy of two tasks. Our unified architecture enables multi-task training: generation loss \mathcal{L}_{gen} and reconstruction loss \mathcal{L}_{rec} . However, according to Table 1 and 2, \mathcal{L}_{gen} does not have a significant positive impact on camera pose estimation, while in Table 3, \mathcal{L}_{rec} also has mixed impact on generation. Thus, we conclude that *we do not observe a synergistic effect between two tasks*, at least in the framework of OpenSora 1.0.

Role of \mathcal{L}_{gen} . Despite two tasks have no observable synergistic effect, we choose to enable \mathcal{L}_{gen} in our full method because it leads to on-par camera pose estimation results (Table 1 and 2) and improved generation quality (Table 3).

Value of JOG3R. To our knowledge, JOG3R is the first method that performs video generation and camera pose estimation jointly. The new unified architecture enables end-to-end training of two tasks, and it opens up new research directions. Without precedents, we can only compare with

state-of-the-art methods in each task, which are dedicated specifically to solve the corresponding tasks. Nonetheless, we still achieve on-par quantitative results in RealEstate10k (Table 1), and all qualitative figures confirm that JOG3R generates realistic videos (T2V), estimates reasonably good camera paths (V2C) and they are self coherent (T2V+C).

5. Conclusions and Future Work

We have presented a thorough analysis on probing the 3D awareness of the intermediate features of a video generation model via the 3D camera pose estimation tasks. In addition to this analysis, we have presented JOG3R, the first unified framework for text-to-video generation (T2V), joint generation and camera estimation (T2V+C), and camera estimation for real videos (V2C).

Since it is not trivial to obtain accurate camera annotations for dynamic scenes, our analysis is limited to videos of static scenes only. It is a promising future direction to analyze how video generation features adapt to camera estimation for dynamic scenes. The length of the video sequences our method can handle is currently limited by the number of frames the generator can synthesize. Handling longer sequences may require adopting sliding window solutions. As the video generators continue to improve to enable generation of longer sequences, our proposed solutions will also naturally extend to handling longer videos with larger baseline.

References

- [1] Sameer Agarwal, Yasutaka Furukawa, Noah Snavely, Ian Simon, Brian Curless, Steven M. Seitz, and Richard Szeliski. Building rome in a day. *2009 IEEE 12th International Conference on Computer Vision*, pages 72–79, 2009. 2
- [2] Max Bain, Arsha Nagrani, Gül Varol, and Andrew Zisserman. Frozen in time: A joint video and image encoder for end-to-end retrieval. In *ICCV*, 2021. 1
- [3] Omer Bar-Tal, Hila Chefer, Omer Tov, Charles Herrmann, Roni Paiss, Shiran Zada, Ariel Ephrat, Junhwa Hur, Yuanzhen Li, Tomer Michaeli, et al. Lumiere: A space-time diffusion model for video generation. *arXiv preprint arXiv:2401.12945*, 2024. 2
- [4] Shariq Farooq Bhat, Reiner Birkl, Diana Wofk, Peter Wonka, and Matthias Müller. ZoeDepth: Zero-shot transfer by combining relative and metric depth. *arXiv*, 2023. 5
- [5] Andreas Blattmann, Tim Dockhorn, Sumith Kulal, Daniel Mendelevitch, Maciej Kilian, Dominik Lorenz, Yam Levi, Zion English, Vikram Voleti, Adam Letts, et al. Stable video diffusion: Scaling latent video diffusion models to large datasets. *arXiv preprint arXiv:2311.15127*, 2023. 1, 2
- [6] Andreas Blattmann, Robin Rombach, Huan Ling, Tim Dockhorn, Seung Wook Kim, Sanja Fidler, and Karsten Kreis. Align your latents: High-resolution video synthesis with latent diffusion models. In *CVPR*, pages 22563–22575, 2023. 2
- [7] Tim Brooks, Bill Peebles, Connor Holmes, Will DePue, Yufei Guo, Li Jing, David Schnurr, Joe Taylor, Troy Luhman, Eric Luhman, Clarence Ng, Ricky Wang, and Aditya Ramesh. Video generation models as world simulators. 2024. 1, 2, 3
- [8] Matthew A. Brown, Gang Hua, and Simon A. J. Winder. Discriminative learning of local image descriptors. *IEEE Transactions on Pattern Analysis and Machine Intelligence*, 33: 43–57, 2011. 2
- [9] Junhao Cai, Yisheng He, Weihao Yuan, Siyu Zhu, Zilong Dong, Liefeng Bo, and Qifeng Chen. Open-vocabulary category-level object pose and size estimation. *IEEE Robotics and Automation Letters*, 2024. 3
- [10] Qi Cai, Lilian Zhang, Yuanxin Wu, Wenxian Yu, and Dewen Hu. A pose-only solution to visual reconstruction and navigation. *IEEE Transactions on Pattern Analysis and Machine Intelligence*, 45(1):73–86, 2021. 2
- [11] Shoufa Chen, Mengmeng Xu, Jiawei Ren, Yuren Cong, Sen He, Yanping Xie, Animesh Sinha, Ping Luo, Tao Xiang, and Juan-Manuel Perez-Rua. Gentron: Delving deep into diffusion transformers for image and video generation. *arXiv preprint arXiv:2312.04557*, 2023. 2
- [12] Tsai-Shien Chen, Aliaksandr Siarohin, Willi Menapace, Ekaterina Deyneka, Hsiang-wei Chao, Byung Eun Jeon, Yuwei Fang, Hsin-Ying Lee, Jian Ren, Ming-Hsuan Yang, and Sergey Tulyakov. Panda-70M: Captioning 70m videos with multiple cross-modality teachers. In *CVPR*, pages 13320–13331, 2024. 1
- [13] David J Crandall, Andrew Owens, Noah Snavely, and Daniel P Huttenlocher. Sfm with mrfs: Discrete-continuous optimization for large-scale structure from motion. *IEEE transactions on pattern analysis and machine intelligence*, 35(12):2841–2853, 2012. 2
- [14] Hainan Cui, Xiang Gao, Shuhan Shen, and Zhanyi Hu. Hsfm: Hybrid structure-from-motion. In *CVPR*, pages 1212–1221, 2017. 2
- [15] Prafulla Dhariwal and Alexander Nichol. Diffusion models beat gans on image synthesis. *Advances in neural information processing systems*, 34:8780–8794, 2021. 2
- [16] Alexey Dosovitskiy, Lucas Beyer, Alexander Kolesnikov, Dirk Weissenborn, Xiaohua Zhai, Thomas Unterthiner, Mostafa Dehghani, Matthias Minderer, Georg Heigold, Sylvain Gelly, et al. An image is worth 16x16 words: Transformers for image recognition at scale. In *ICLR*, 2021. 3
- [17] Niladri Shekhar Dutt, Sanjeev Muralikrishnan, and Niloy J Mitra. Diffusion 3d features (diff3f): Decorating untextured shapes with distilled semantic features. In *CVPR*, pages 4494–4504, 2024. 1, 3
- [18] Mohamed El Banani, Amit Raj, Kevis-Kokitsi Maninis, Abhishek Kar, Yuanzhen Li, Michael Rubinstein, Deqing Sun, Leonidas Guibas, Justin Johnson, and Varun Jampani. Probing the 3d awareness of visual foundation models. In *CVPR*, pages 21795–21806, 2024. 1, 3
- [19] Martin A Fischler and Robert C Bolles. Random sample consensus: a paradigm for model fitting with applications to image analysis and automated cartography. *Communications of the ACM*, 24(6):381–395, 1981. 3

- [20] Haoyu Guo, Sida Peng, Haotong Lin, Qianqian Wang, Guofeng Zhang, Hujun Bao, and Xiaowei Zhou. Neural 3d scene reconstruction with the manhattan-world assumption. In *CVPR*, pages 5501–5510, 2022. 2
- [21] Yuwei Guo, Ceyuan Yang, Anyi Rao, Zhengyang Liang, Yaohui Wang, Yu Qiao, Maneesh Agrawala, Dahua Lin, and Bo Dai. AnimateDiff: Animate your personalized text-to-image diffusion models without specific tuning. In *ICLR*, 2024. 1
- [22] Michal Havlena and Konrad Schindler. Vocmatch: Efficient multiview correspondence for structure from motion. In *ECCV*, 2014. 2
- [23] Hao He, Yinghao Xu, Yuwei Guo, Gordon Wetzstein, Bo Dai, Hongsheng Li, and Ceyuan Yang. CameraCtrl: Enabling camera control for text-to-video generation. *arXiv preprint arXiv:2404.02101*, 2024. 5
- [24] Yingqing He, Tianyu Yang, Yong Zhang, Ying Shan, and Qifeng Chen. Latent video diffusion models for high-fidelity long video generation. *arXiv preprint arXiv:2211.13221*, 2022. 2
- [25] Eric Hedlin, Gopal Sharma, Shweta Mahajan, Hossam Isack, Abhishek Kar, Andrea Tagliasacchi, and Kwang Moo Yi. Unsupervised semantic correspondence using stable diffusion. In *NeurIPS*, 2024. 3
- [26] Martin Heusel, Hubert Ramsauer, Thomas Unterthiner, Bernhard Nessler, and Sepp Hochreiter. GANs trained by a two time-scale update rule converge to a local nash equilibrium. *NeurIPS*, 2017. 6
- [27] Jonathan Ho, Ajay Jain, and Pieter Abbeel. Denoising diffusion probabilistic models. In *NeurIPS*, pages 6840–6851, 2020. 2
- [28] Jonathan Ho, William Chan, Chitwan Saharia, Jay Whang, Ruiqi Gao, Alexey Gritsenko, Diederik P Kingma, Ben Poole, Mohammad Norouzi, David J Fleet, et al. Imagen video: High definition video generation with diffusion models. *arXiv preprint arXiv:2210.02303*, 2022. 2
- [29] Jonathan Ho, Tim Salimans, Alexey Gritsenko, William Chan, Mohammad Norouzi, and David J Fleet. Video diffusion models. In *NeurIPS*, pages 8633–8646, 2022. 2
- [30] Aleksander Holynski, David Geraghty, Jan-Michael Frahm, Chris Sweeney, and Richard Szeliski. Reducing drift in structure from motion using extended features. In *2020 International Conference on 3D Vision (3DV)*, pages 51–60. IEEE, 2020. 2
- [31] Hanwen Jiang, Arjun Karpur, Bingyi Cao, Qixing Huang, and André Araujo. OmniGlue: Generalizable feature matching with foundation model guidance. In *CVPR*, pages 19865–19875, 2024. 3
- [32] Nianjuan Jiang, Zhaopeng Cui, and Ping Tan. A global linear method for camera pose registration. In *ICCV*, pages 481–488, 2013. 2
- [33] Vincent Lepetit, Francesc Moreno-Noguer, and Pascal Fua. Ep n p: An accurate o (n) solution to the p n p problem. *IJCV*, 81:155–166, 2009. 3
- [34] Vincent Leroy, Yohann Cabon, and Jerome Revaud. Grounding image matching in 3d with mast3r, 2024. 3
- [35] Dongxu Li, Junnan Li, Hung Le, Guangsen Wang, Silvio Savarese, and Steven C.H. Hoi. LAVIS: A one-stop library for language-vision intelligence. In *Proceedings of the 61st Annual Meeting of the Association for Computational Linguistics (Volume 3: System Demonstrations)*, pages 31–41, Toronto, Canada, 2023. Association for Computational Linguistics. 5
- [36] Zhaoshuo Li, Thomas Müller, Alex Evans, Russell H Taylor, Mathias Unberath, Ming-Yu Liu, and Chen-Hsuan Lin. Neuralangelo: High-fidelity neural surface reconstruction. In *CVPR*, pages 8456–8465, 2023. 2
- [37] Philipp Lindenberger, Paul-Edouard Sarlin, Viktor Larsson, and Marc Pollefeys. Pixel-perfect structure-from-motion with featuremetric refinement. In *ICCV*, pages 5987–5997, 2021. 2
- [38] Lu Ling, Yichen Sheng, Zhi Tu, Wentian Zhao, Cheng Xin, Kun Wan, Lantao Yu, Qianyu Guo, Zixun Yu, Yawen Lu, et al. DL3DV-10K: A large-scale scene dataset for deep learning-based 3d vision. In *CVPR*, pages 22160–22169, 2024. 5
- [39] Yin Lou, Noah Snaveley, and Johannes Gehrke. MatchMiner: Efficient spanning structure mining in large image collections. In *ECCV*, 2012. 2
- [40] David G. Lowe. Distinctive image features from scale-invariant keypoints. *IJCV*, 60:91–110, 2004. 2
- [41] Bin Luo and Edwin R. Hancock. Procrustes alignment with the em algorithm. In *Computer Analysis of Images and Patterns*, pages 623–631, Berlin, Heidelberg, 1999. Springer Berlin Heidelberg. 3
- [42] Xin Ma, Yaohui Wang, Gengyun Jia, Xinyuan Chen, Ziwei Liu, Yuan-Fang Li, Cunjian Chen, and Yu Qiao. Latte: Latent diffusion transformer for video generation. *arXiv preprint arXiv:2401.03048*, 2024. 2, 3, 5
- [43] Zeyu Ma, Zachary Teed, and Jia Deng. Multiview stereo with cascaded epipolar raft. In *ECCV*, pages 734–750. Springer, 2022. 2
- [44] Willi Menapace, Aliaksandr Siarohin, Ivan Skorokhodov, Ekaterina Deyneka, Tsai-Shien Chen, Anil Kag, Yuwei Fang, Aleksei Stoliar, Elisa Ricci, Jian Ren, et al. Snap video: Scaled spatiotemporal transformers for text-to-video synthesis. In *CVPR*, pages 7038–7048, 2024. 1, 2
- [45] Zak Murez, Tarrence van As, James Bartolozzi, Ayan Sinha, Vijay Badrinarayanan, and Andrew Rabinovich. Atlas: End-to-end 3d scene reconstruction from posed images. In *ECCV*, 2020. 2
- [46] Michael Oechsle, Songyou Peng, and Andreas Geiger. UNISURF: Unifying neural implicit surfaces and radiance fields for multi-view reconstruction. In *ICCV*, pages 5569–5579, 2021. 2
- [47] Evin Pinar Örnek, Yann Labbé, Bugra Tekin, Lingni Ma, Cem Keskin, Christian Forster, and Tomas Hodan. Foundpose: Unseen object pose estimation with foundation features. *arXiv preprint arXiv:2311.18809*, 2023. 3
- [48] Linfei Pan, Dániel Baráth, Marc Pollefeys, and Johannes Lutz Schönberger. Global structure-from-motion revisited. In *ECCV*, 2024. 2, 5, 6, 7, 8
- [49] William Peebles and Saining Xie. Scalable diffusion models with transformers. In *ICCV*, pages 4195–4205, 2023. 2, 3

- [50] Rui Peng, Xiaodong Gu, Luyang Tang, Shihe Shen, Fanqi Yu, and Ronggang Wang. GenS: Generalizable neural surface reconstruction from multi-view images. In *NeurIPS*, 2023. 2
- [51] Colin Raffel, Noam Shazeer, Adam Roberts, Katherine Lee, Sharan Narang, Michael Matena, Yanqi Zhou, Wei Li, and Peter J Liu. Exploring the limits of transfer learning with a unified text-to-text transformer. *Journal of machine learning research*, 21(140):1–67, 2020. 5
- [52] René Ranftl, Alexey Bochkovskiy, and Vladlen Koltun. Vision transformers for dense prediction. In *ICCV*, pages 12159–12168, 2021. 3
- [53] Robin Rombach, Andreas Blattmann, Dominik Lorenz, Patrick Esser, and Björn Ommer. High-resolution image synthesis with latent diffusion models. In *CVPR*, 2021. 1, 2, 5
- [54] Mohamed Sayed, John Gibson, Jamie Watson, Victor Adrian Prisacariu, Michael Firman, and Clément Godard. Simplerecon: 3d reconstruction without 3d convolutions. In *ECCV*, 2022. 2
- [55] Johannes L Schonberger and Jan-Michael Frahm. Structure-from-motion revisited. In *CVPR*, pages 4104–4113, 2016. 2
- [56] Johannes L Schönberger, Enliang Zheng, Jan-Michael Frahm, and Marc Pollefeys. Pixelwise view selection for unstructured multi-view stereo. In *ECCV*, pages 501–518. Springer, 2016. 2
- [57] Uriel Singer, Adam Polyak, Thomas Hayes, Xi Yin, Jie An, Songyang Zhang, Qiyuan Hu, Harry Yang, Oron Ashual, Oran Gafni, et al. Make-a-video: Text-to-video generation without text-video data. *arXiv preprint arXiv:2209.14792*, 2022. 2
- [58] Yang Song, Jascha Sohl-Dickstein, Diederik P Kingma, Abhishek Kumar, Stefano Ermon, and Ben Poole. Score-based generative modeling through stochastic differential equations. *arXiv preprint arXiv:2011.13456*, 2020. 2
- [59] Jiaming Sun, Xi Chen, Qianqian Wang, Zhengqi Li, Hadar Averbuch-Elor, Xiaowei Zhou, and Noah Snavely. Neural 3d reconstruction in the wild. In *ACM SIGGRAPH 2022 conference proceedings*, pages 1–9, 2022. 2
- [60] Luming Tang, Menglin Jia, Qianqian Wang, Cheng Perng Phoo, and Bharath Hariharan. Emergent correspondence from image diffusion. In *NeurIPS*, 2023. 1, 3, 4
- [61] Zachary Teed and Jia Deng. Deepv2d: Video to depth with differentiable structure from motion. *ArXiv*, abs/1812.04605, 2018. 3
- [62] Benjamin Ummenhofer and Vladlen Koltun. Adaptive surface reconstruction with multiscale convolutional kernels. In *ICCV*, pages 5651–5660, 2021. 2
- [63] Benjamin Ummenhofer, Huizhong Zhou, Jonas Uhrig, Nikolaus Mayer, Eddy Ilg, Alexey Dosovitskiy, and Thomas Brox. DeMoN: Depth and motion network for learning monocular stereo. In *CVPR*, pages 5622–5631, 2016. 3
- [64] Thomas Unterthiner, Sjoerd van Steenkiste, Karol Kurach, Raphaël Marinier, Marcin Michalski, and Sylvain Gelly. FVD: A new metric for video generation. In *ICLR workshop*, 2019. 6
- [65] Sheng Wan, Tung-Yu Wu, Wing H. Wong, and Chen-Yi Lee. Confnet: Predict with confidence. In *2018 IEEE International Conference on Acoustics, Speech and Signal Processing (ICASSP)*, pages 2921–2925, 2018. 4
- [66] Jianyuan Wang, Christian Ruppert, and David Novotny. Posediffusion: Solving pose estimation via diffusion-aided bundle adjustment. In *ICCV*, pages 9773–9783, 2023. 5
- [67] Jiuniu Wang, Hangjie Yuan, Dayou Chen, Yingya Zhang, Xiang Wang, and Shiwei Zhang. Modelscope text-to-video technical report. *arXiv preprint arXiv:2308.06571*, 2023. 2
- [68] Peng Wang, Lingjie Liu, Yuan Liu, Christian Theobalt, Taku Komura, and Wenping Wang. Neus: Learning neural implicit surfaces by volume rendering for multi-view reconstruction. *ArXiv*, abs/2106.10689, 2021. 2
- [69] Shuzhe Wang, Vincent Leroy, Yohann Cabon, Boris Chidlovskii, and Jerome Revaud. Dust3r: Geometric 3d vision made easy. In *CVPR*, 2024. 1, 2, 3, 4, 5, 6, 7
- [70] Yiqun Wang, Ivan Skorokhodov, and Peter Wonka. Improved surface reconstruction using high-frequency details. *ArXiv*, abs/2206.07850, 2022. 2
- [71] Yaohui Wang, Xinyuan Chen, Xin Ma, Shangchen Zhou, Ziqi Huang, Yi Wang, Ceyuan Yang, Yanan He, Jiashuo Yu, Peiqing Yang, et al. LaviE: High-quality video generation with cascaded latent diffusion models. *arXiv preprint arXiv:2309.15103*, 2023. 2
- [72] Philippe Weinzaepfel, Vincent Leroy, Thomas Lucas, Romain Brégier, Yohann Cabon, Vaibhav ARORA, Leonid Antsfeld, Boris Chidlovskii, Gabriela Csurka, and Jerome Revaud. Croco: Self-supervised pre-training for 3d vision tasks by cross-view completion. In *NeurIPS*, 2022. 3
- [73] Bernhard P. Wrobel. Multiple view geometry in computer vision. *Künstliche Intell.*, 15:41, 2001. 2
- [74] Changchang Wu. Towards linear-time incremental structure from motion. *2013 International Conference on 3D Vision*, pages 127–134, 2013. 2
- [75] Jay Zhangjie Wu, Yixiao Ge, Xintao Wang, Stan Weixian Lei, Yuchao Gu, Yufei Shi, Wynne Hsu, Ying Shan, Xiaohu Qie, and Mike Zheng Shou. Tune-a-video: One-shot tuning of image diffusion models for text-to-video generation. In *ICCV*, pages 7623–7633, 2023. 2
- [76] Guangkai Xu, Wei Yin, Hao Chen, Chunhua Shen, Kai Cheng, and Feng Zhao. Frozenrecon: Pose-free 3d scene reconstruction with frozen depth models. In *ICCV*, pages 9276–9286. IEEE, 2023. 3
- [77] Xinyi Ye, Weiyue Zhao, Tianqi Liu, Zihao Huang, Zhiguo Cao, and Xin Li. Constraining depth map geometry for multi-view stereo: A dual-depth approach with saddle-shaped depth cells. In *ICCV*, pages 17661–17670, 2023. 2
- [78] Zhichao Yin and Jianping Shi. Geonet: Unsupervised learning of dense depth, optical flow and camera pose. In *CVPR*, pages 1983–1992, 2018. 3
- [79] Zehao Yu, Songyou Peng, Michael Niemeyer, Torsten Sattler, and Andreas Geiger. Monosdf: Exploring monocular geometric cues for neural implicit surface reconstruction. *ArXiv*, abs/2206.00665, 2022. 2
- [80] Yuanwen Yue, Anurag Das, Francis Engelmann, Siyu Tang, and Jan Eric Lenssen. Improving 2d feature representations

- by 3d-aware fine-tuning. *arXiv preprint arXiv:2407.20229*, 2024. 3
- [81] Guanqi Zhan, Chuanxia Zheng, Weidi Xie, and Andrew Zisserman. What does stable diffusion know about the 3d scene? *arXiv preprint arXiv:2310.06836*, 2023. 3
- [82] David Junhao Zhang, Jay Zhangjie Wu, Jia-Wei Liu, Rui Zhao, Lingmin Ran, Yuchao Gu, Difei Gao, and Mike Zheng Shou. Show-1: Marrying pixel and latent diffusion models for text-to-video generation. *arXiv preprint arXiv:2309.15818*, 2023. 2
- [83] Junyi Zhang, Charles Herrmann, Junhwa Hur, Luisa Polania Cabrera, Varun Jampani, Deqing Sun, and Ming-Hsuan Yang. A tale of two features: Stable diffusion complements DINO for zero-shot semantic correspondence. In *NeurIPS*, 2023. 3
- [84] Junyi Zhang, Charles Herrmann, Junhwa Hur, Eric Chen, Varun Jampani, Deqing Sun, and Ming-Hsuan Yang. Telling left from right: Identifying geometry-aware semantic correspondence. In *CVPR*, pages 3076–3085, 2024. 3
- [85] Zhe Zhang, Rui Peng, Yuxi Hu, and Ronggang Wang. Geomvsnet: Learning multi-view stereo with geometry perception. In *CVPR*, pages 21508–21518, 2023. 2
- [86] Wenliang Zhao, Yongming Rao, Zuyan Liu, Benlin Liu, Jie Zhou, and Jiwen Lu. Unleashing text-to-image diffusion models for visual perception. In *ICCV*, 2023. 3
- [87] Zangwei Zheng, Xiangyu Peng, Tianji Yang, Chenhui Shen, Shenggui Li, Hongxin Liu, Yukun Zhou, Tianyi Li, and Yang You. Open-sora: Democratizing efficient video production for all, 2024. 1, 2, 3
- [88] Huizhong Zhou, Benjamin Ummenhofer, and Thomas Brox. DeepTAM: Deep tracking and mapping with convolutional neural networks. *IJCV*, 128:756 – 769, 2019. 3
- [89] Tinghui Zhou, Richard Tucker, John Flynn, Graham Fyffe, and Noah Snavely. Stereo magnification: Learning view synthesis using multiplane images. *arXiv preprint arXiv:1805.09817*, 2018. 5

Appendices

The supplementary material of submission consists of this document and the webpage.

A. Temporal smoothness term

Given the estimated camera pose $(\mathbf{R}_f, \mathbf{t}_f)$ and focal length l_f for each frame f , we define \mathcal{L}_{fl} and $\mathcal{L}_{\text{transl}}$ as below:

$$\mathcal{L}_{\text{fl}} = \sum_f \|l_f - l_{f+1}\|_2^2 \quad (3)$$

$$\mathcal{L}_{\text{transl}} = \sum_f \|\mathbf{t}_f - \mathbf{t}_{f+1}\|_2^2 + \|\mathbf{v}_f - \mathbf{v}_{f+1}\|_2^2 \quad (4)$$

where $\mathbf{v}_f = \mathbf{t}_f - \mathbf{t}_{f+1}$. The first term of $\mathcal{L}_{\text{transl}}$ encourages static camera position while the second term encourages constant velocity.

B. Architectural design choice

In Table 1 below, we compare the quality of estimated camera poses using the feature maps in different DiT block b^i . Row 1c and 2c correspond respectively to our full JOG3R model (row 1c in Table 1 and 2 in the main paper), which is $i=26$. We first confirm using the features one block later, $i=27$, does not result in significant difference (row 1d vs. 1c; 2d vs. 2c). Next, we consider $i=10$ and 20, representing approximately one-third and two-third of total DiT blocks. We see that compared to our results in the main paper (row 1c and 2c), $i=10$ yields lower errors in RealEstate10k-test but higher errors in DL3DV10k (row 1a and 2a), suggesting that using features of earlier blocks has a higher risk of poor generalization. Meanwhile, $i=20$ attains the lowest errors in both datasets, while ours remains on-par. We therefore conclude that *features of later blocks, e.g., $i \in [20, 27]$ is preferred than earlier blocks, and all later blocks should lead to similar results*. Instead of solely relying on one block b^i , one can potentially devise a module fusing features of all DiT blocks and projecting to the input space of DUST3R decoders, which we consider future work.

Backbone / Method	b^i	Rot. err. ($^\circ$) \downarrow	Transl. err. ($^\circ$) \downarrow	RRA@5 $^\circ$ \uparrow	RTA@5 $^\circ$ \uparrow	mAA@30 $^\circ$ \uparrow
RealEstate10k						
1a. trainable DiT	b^{10}	0.28	18.94	99.94%	18.75%	52.63%
1b. trainable DiT	b^{20}	0.28	19.10	99.85%	21.59%	53.35%
1c. trainable DiT	b^{26} (JOG3R)	0.29	22.15	99.79%	19.18%	47.25%
1d. trainable DiT	b^{27}	0.28	23.09	99.80%	17.74%	46.88%
DL3DV10k						
2a. trainable DiT	b^{10}	4.68	30.90	73.87%	6.08%	30.76%
2b. trainable DiT	b^{20}	4.01	27.71	77.91%	10.56%	36.62%
2c. trainable DiT	b^{26} (JOG3R)	4.20	29.17	78.63%	7.86%	34.22%
2d. trainable DiT	b^{27}	4.65	30.36	77.15%	7.98%	32.86%

Table 4. **Ablation study on which feature maps b^i get passed to DUST3R.** Row 1c and 2c correspond respectively to our full JOG3R model (row 1c in Table 1 and 2 in the main paper).